Chapter 6: Optimization of post-sintering parameters for fabricating advanced HP-Cu current collectors

This chapter provides a comprehensive account of the optimization of post-sintering parameters aimed at enhancing the performance of Cu current collectors specifically developed for LMB applications. It begins by systematic and methodical optimization of sintering parameters and the successful fabrication of a high-strength porous Cu current collector featuring a pore size of less than 200 μm. The chapter details a series of carefully designed experiments that explore the influence of critical sintering variables, namely sintering temperature, heating rate, and soaking time on key material properties such as relative density, compressive strength, and volumetric shrinkage. These output parameters are crucial indicators of the mechanical and structural integrity of the fabricated current collectors. The chapter further elaborates on the experimental methodology, which includes detailed morphological characterization used to assess the microstructure and physical attributes of the porous Cu structures. This systematic investigation enabled the identification of an optimal combination of sintering parameters that yield superior mechanical and structural performance. In addition to the parameter optimization, the chapter also presents a preliminary study on the compression behavior and electrochemical performance of the fabricated Cu current collectors. This segment of the research offers practical insights into the functional applicability of the optimized current collectors, particularly those with sub-200 μm pore sizes. Overall, the chapter establishes a strong foundation for the targeted design and fabrication of porous Cu current collectors and offers significant contributions to the advancement of material processing techniques in the field of energy storage systems.

Moreover, this research represents a significant advancement in the field of porous Cu current collectors for energy storage devices. It not only establishes a robust framework for the systematic optimization of sintering parameters but also sets a benchmark for the fabrication and application of high-strength, finely porous Cu current collectors, thereby contributing to the broader field of energy storage technology development.

6.1 Results and Discussion

6.1.1 Sintering Mechanism

The sintering process involves multiple diffusion mechanisms, primarily grain boundary and lattice diffusion, each dominating at different temperature ranges. At intermediate temperatures (~650–800 °C), grain boundary diffusion is the dominant mechanism. In this stage, atoms migrate along grain boundaries, leading to initial neck growth between copper particles and moderate densification without significant grain growth. As the sintering temperature increases beyond 850 °C, lattice (volume) diffusion becomes more significant. This mechanism involves atomic movement through the bulk of the grains, contributing to further densification and grain coarsening.

Therefore, it is crucial to investigate the sintering behavior of these green Cu samples. Sintering facilitates the bonding of particles, driven by a reduction in surface energy due to the high surface area of the particles. The Cu particles used are small (1-3 μm) and nearly spherical which means that there is a significant driving force for sintering, enabling particle bonding even without external compaction or pressure. Fig. 6.1 illustrates the effect of temperature during sintering on Cu particle bonding. Sintering typically involves three main stages: neck formation, rounding of pore, and initiation of grain growth, followed by pores collapse resulting in the formation of closed spheres [115]. At 650°C, (Fig. 6.1 a), neck formation between Cu particles is visible, but the pores and voids that are present, are larger in number. The grain growth and pore collapse occur with the increase in

temperature. At 1050°C, the porosity in the Cu samples is notably reduced compared to those processed at lower temperatures, as shown in Fig. 6.1 (d) and 6.1 (e).

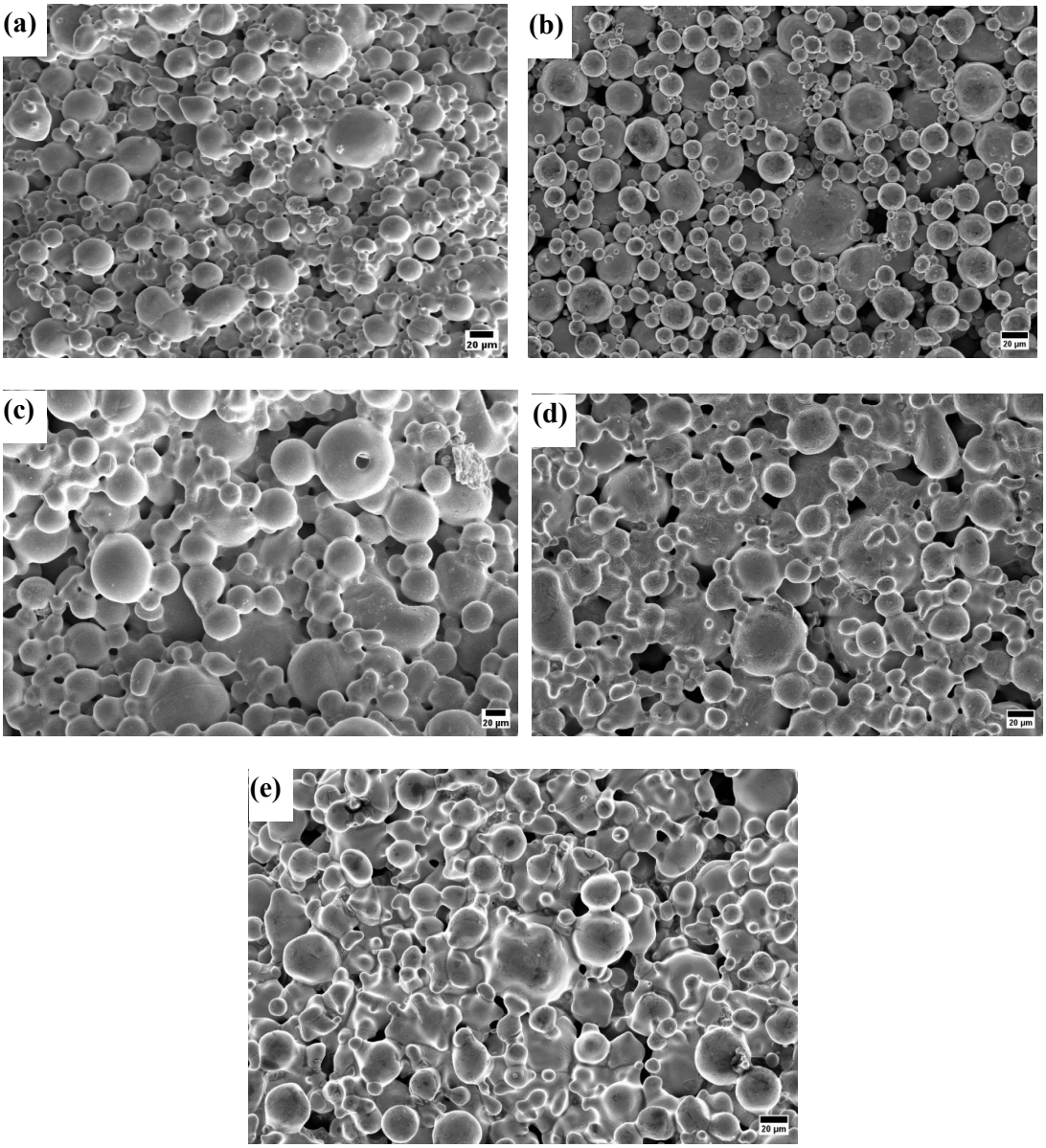

Fig. 6.1: SEM images of Cu samples prepared at different sintering temperature i.e. (a) 650℃ (b) 750℃ (c) 850℃ (d) 950℃ (e) 1050℃

Previous studies [63] indicate that sintering of pure Cu at lower temperatures (650-750°C) is primarily governed by surface diffusion mechanisms. In contrast, at higher temperatures (greater than 850°C), the more prominent mechanisms are grain boundary diffusion and

volume diffusion. This is evident in Fig. 6.1, in comparison to Cu samples sintered at lower temperatures, those sintered at higher temperatures exhibit denser and more isolated round pores.

6.1.2 Process parameters effects on relative density

Fig. 6.2 (a) represents the main effect plot for the relative density. The effect of the sintering temperature on the relative density has been discussed in subsequent sub- sections.

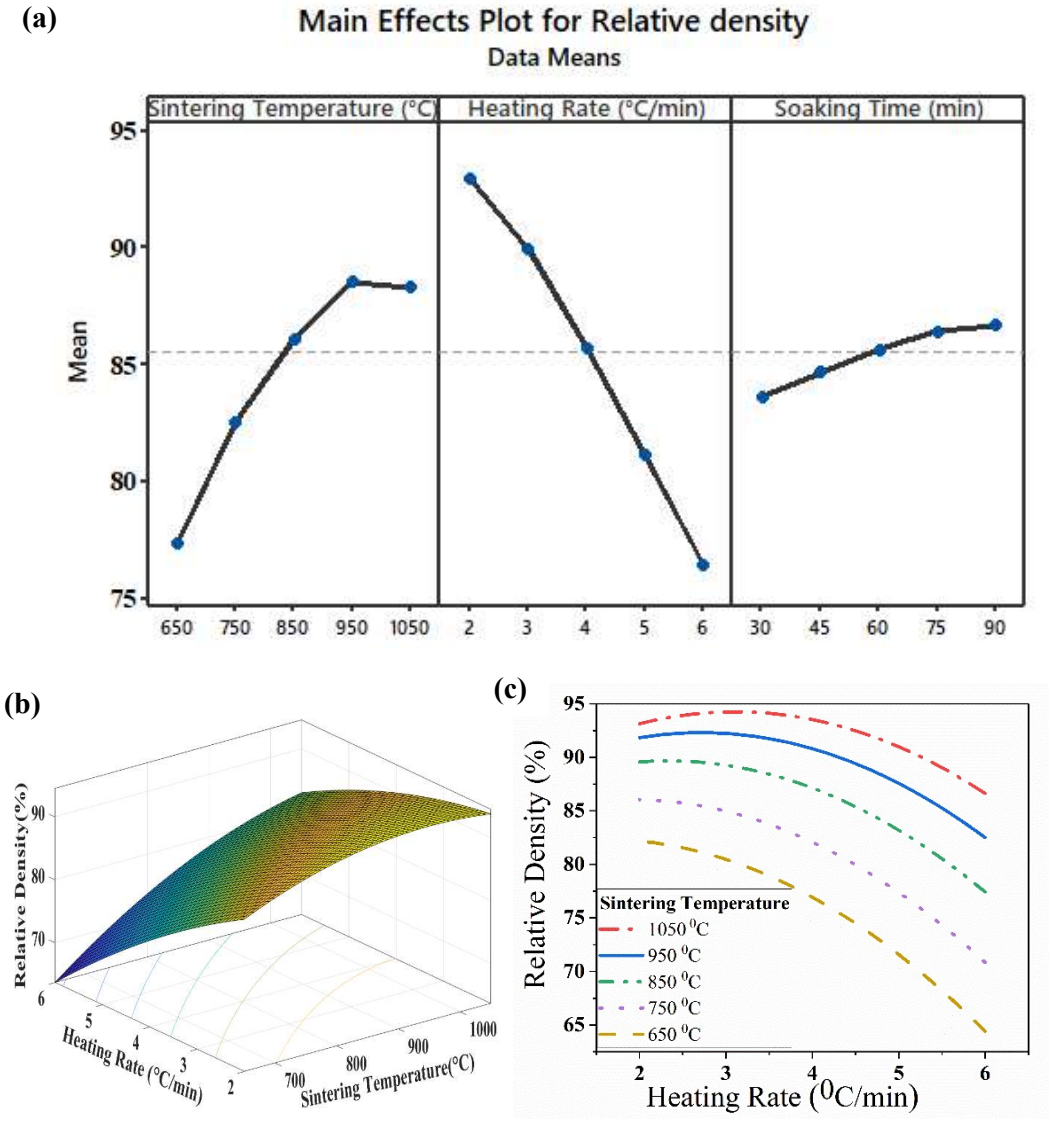

Fig. 6.2: a) Main effect plot and (b-c) Interaction plot for relative density

6.1.2.1 Effect of temperature

The relative density is found to increase with increasing sintering temperature as evident from Fig. 6.2 (a) up to 950 ℃ beyond which it is observed to stabilize. The reason for low relative density at lower temperatures could be attributed to dominant surface diffusion mechanism. As previously indicated, when the sintering temperature is maintained below 750 °C, the dominant mechanism facilitating particle bonding and neck formation is surface diffusion. Surface diffusion primarily contributes to the initial stages of sintering by enabling atom migration along the particle surfaces, which promotes neck growth between adjacent particles. However, this mechanism does not contribute significantly to densification, as it does not facilitate substantial mass transport into the pore regions. As a result, sintering at lower temperatures primarily results in particle coalescence without a marked reduction in porosity.

On the other hand, true densification in sintering processes is largely driven by volume diffusion and grain boundary diffusion, which become more active at elevated temperatures. When the sintering temperature is increased beyond 750 °C, these bulk diffusion mechanisms begin to dominate. Volume diffusion involves the migration of atoms from the interior of the particles into the neck region and into void spaces, which leads to pore shrinkage and an overall reduction in porosity. Similarly, grain boundary diffusion enables atoms to move along grain interfaces, enhancing the consolidation of particles and contributing further to densification.

Consequently, as the sintering temperature crosses the 750 °C threshold, a significant transition in the governing diffusion mechanism occurs from surface-dominated diffusion to volume- and grain-boundary-dominated diffusion. This transition results in a more pronounced increase in the material's relative density, as the microstructure becomes more compact and voids between particles are reduced. The experimental observations align well

with this theoretical understanding, confirming that higher sintering temperatures promote more effective densification through enhanced atomic mobility and deeper mass transport into the porous structure.

Furthermore, after 950 ℃, there was almost no increase in relative density and it stabilized after that. As densification is governed by reduction in surface energy, thus at high temperature (greater than 950 ℃) the surface energy available for densification gets reduced significantly. Hence, a further increase in temperature may not support further densification [63].

6.1.2.2 Effect of heating rate

The effect of the heating rate on relative density can be observed in the main effect plot as shown in Fig. 6.2 (a). The heating rate was found to significantly affect the relative density as continuous reduction in relative density was observed with the increase in heating rate. At low value of heating rate, sufficient time for diffusion and mass transport between the Cu particle is available resulting in a higher relative density. It has also been reported in previous studies [107] that slow heating results in enhanced homogeneity and controlled sintering. The enhanced homogeneity is the result of better thermal equilibrium that leads to uniform temperature distribution and hence better relative density. These observations are in consonance with previously reported work [63] which shows the reduction in relative density with the increase in heating rate.

6.1.2.3 Effect of soaking time

Fig. 6.2 (a) shows the variation of relative density over the soaking time. It can be observed from Fig. 6.2 (a), that as the soaking time increases, the relative density also increases. The increase in the relative density is due to the amount of time that Cu particles have to migrate and reorient. Moreover, the soaking time also affects the neck formation and grain growth in the Cu particles having different sizes [116], [117]. It can be observed from the Fig. 6.6

that Cu particles having a small diameter were forming strong bonds due to a fast diffusion rate as compared to large-shaped Cu particles for the 30 min of soaking time. For the soaking time of 90 min, small and large size Cu particles both are diffused properly, and the formation of strong bonds takes place. Hence, it could be inferred that with the increase in soaking time sufficient amount of bonding and growth occurred resulting in an overall increase in relative density.

6.1.2.4 Effect of interaction

The experimental result in Fig. 6.2: (a) shows the surface and the interaction plots between the sintering temperature and the relative density with the increase in the heating rate. It can be observed that the effect of variation in heating rate is more significant at low sintering temperatures as compared to higher values of sintering temperatures. At sintering temperatures $> 1000℃$, the heating rate ranging from 2 to 4 ℃ /min results in similar values of relative densities. This may be attributed to the difference in diffusion mechanism at different levels of sintering temperatures. As discussed already, at low sintering temperatures i.e. $< 850℃$ the dominant mechanism for sintering is surface diffusion, thus variation in the heating rate at low-temperature ranges resulted in variation in the time available for surface diffusion of the particles thereby causing variation in sintered density. On the contrary, at a higher sintering temperature range, the densification occurred mainly due to volumetric diffusion. Also, at higher temperatures and low heating rates, the driving force for sintering reduces drastically as it approaches the limiting density. Thus, at higher sintering temperatures, the effect of variation in heating rate was not that significant. However, for heating rate values higher than 4 ℃ /min this effect was found to be significant as the driving force in such cases may be higher to cause densification.

6.1.3 Effect of process parameters on compressive strength

The effect of various sintering parameters like sintering temperature, soaking time, and heating rate on the compressive strength has been shown in the main effect plot in Fig. 6.3(a). The effect of a single parameter and interaction has been discussed in the further sub-sections.

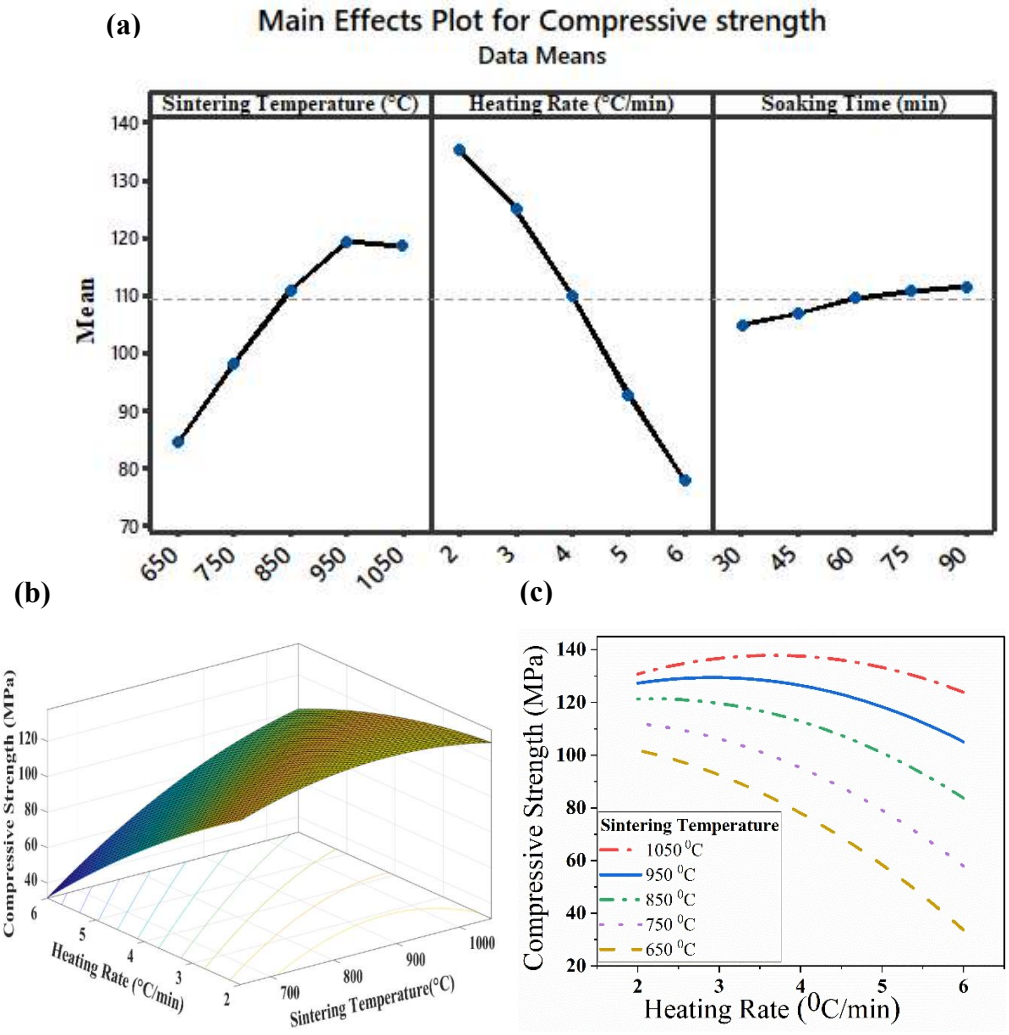

Fig. 6.3: a) Main effect plot and (b-c) Interaction plot for compressive strength.

6.1.3.1 Effect of temperature

It could be inferred from Fig. 6.3 (a) that the variation in compressive strength with respect to sintering temperature followed the same trend as shown by the relative density. Thus, it

could be established that the variation in compressive strength is mainly due to change in the relative density of the samples. It has been reported in previous studies [116] that the rate of particle diffusion increases with the increase in the sintering temperature and this enhancement in the relative density results in the higher compressive strength.

6.1.3.2 Effect of heating rate

The compressive strength of the samples was found to be reduced with the increase in the heating rate. It has been reported in previous studies [116] that a fast-heating rate may cause non-uniform temperature distribution. This non-uniform temperature distribution may result in lower compressive strength. Further, at a low value of heating rates, sufficient time for surface and volumetric diffusion is available that may lead to better bonding between the particles thereby causing increase in compressive strength. At higher heating rate values, the Cu particles spend less time at intermediate temperatures where neck formation and densification are crucial. This can limit the extent of bonding and lead to a reduction in compressive strength.

6.1.3.3 Effect of soaking time

It can be inferred from Fig. 6.3 (a) that with the increase in soaking time, the compressive strength was found to increase till 90 min of soaking. At relatively low soaking time, the diffusion processes, including surface diffusion, volume diffusion, and grain boundary diffusion, may not have sufficient time to proceed to the extent required for thorough densification. Moreover, limited neck growth between particles may occur, resulting in higher residual porosity and consequently reduced compression strength. This effect can be seen clearly from the SEM images (Fig. 6.6) of the samples sintered at 30 min and 90 min of soaking time respectively. Moreover, from Fig. 6.3 (a), it could be observed that compressive strength value after 75 min of soaking time has almost become stagnant with maximum value achieved at 90 min.

6.1.3.4 Effect of interaction

The interaction between the compressive strength and the heating rate has been shown in Fig.6.3 (c). It can be observed from the Fig.6.3 that at high value of sintering temperature and low value of the heating rate, the value of the compressive strength was found to be higher. The high value of the sintering temperature and low values of heating rate contribute to the strong bond formation and high densification between the Cu particles which result in increase in the compressive strength.

6.1.4 Effect of process parameters on volumetric shrinkage

The effect of various parameters on the volumetric shrinkage has been shown in the main effect plot in Fig. 6.4 (a) and the effects of individual parameters have been discussed below.

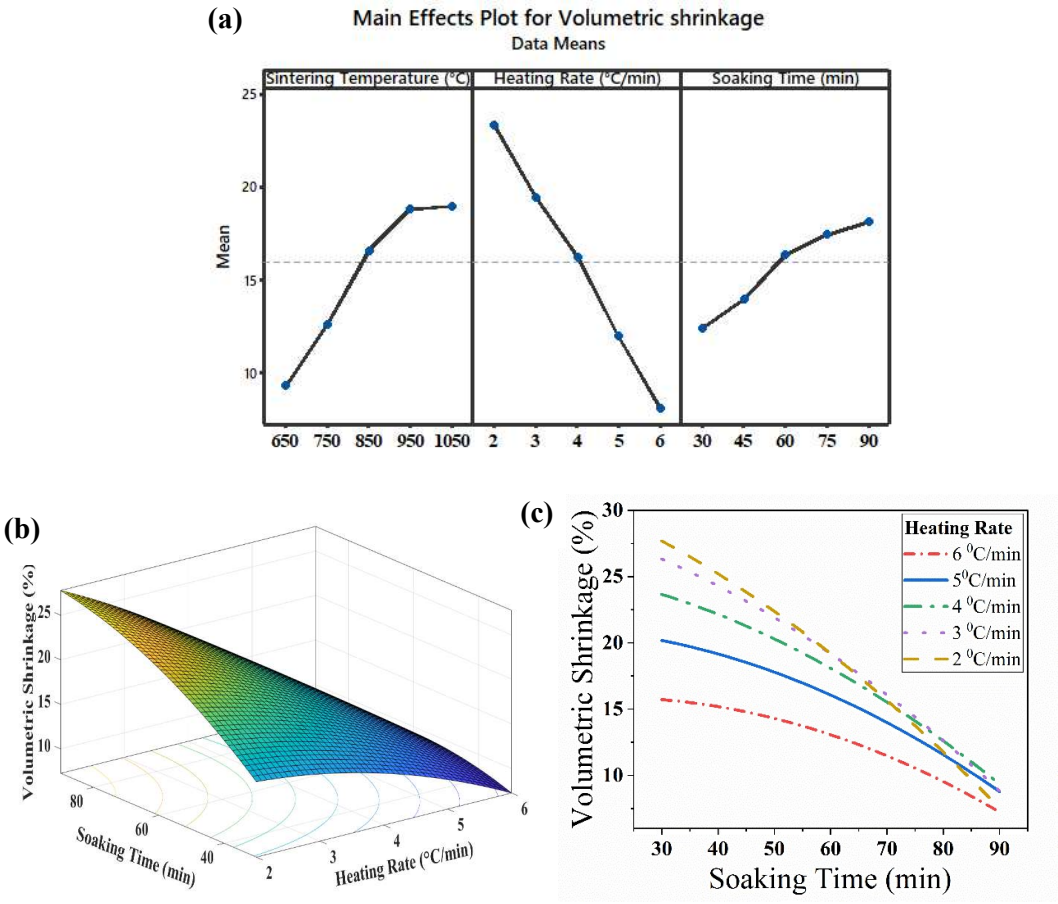

Fig. 6.4: a) Main effect plot and (b-c) Interaction plot for Volumetric Shrinkage

6.1.4.1 Effect of temperature

Sintering temperature has a significant effect on the volumetric shrinkage during the sintering process. With increase in temperature, the Cu particles are pulled towards each other due to the surface energy for the diffusion process. The volumetric shrinkage occurs due to the movement of the Cu particles through the mass conservation process. Moreover, when the Cu particles are sintered at high temperature, the grain boundary and volume diffusion mechanism play a key role in densification. Both the mechanisms result in a high amount of particle merging, reorientation and transport thus leading to high volumetric shrinkage. At low values of sintering temperatures, the rate of atomic diffusion is relatively slow, leading to limited neck formation and minimal particle bonding. As a result, the material exhibits minimal shrinkage because there is insufficient time and energy for significant densification.

6.1.4.2 Effect of heating rate

The heating rate has a severe effect on the volumetric shrinkage. Fig. 6.5 illustrates the morphological characteristics of the samples subjected to sintering at 950 °C for 60 minutes, employing two distinct heating rates: (a) a slow ramp of 2 °C/min and (b) a comparatively faster ramp of 6 °C/min.

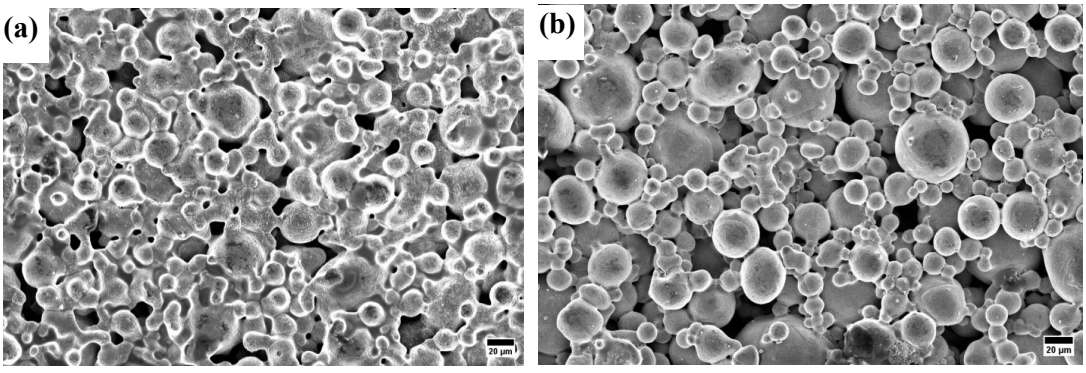

Fig. 6.5: SEM images of the samples sintered at the sintering temperature of 950℃, soaking time of 60 min with heating rate a) 2 ℃/min b) 6 ℃/min.

The reason for this effect could be associated with the energy supplied during the sintering process. When the heating rate was less, the amount of energy that was supplied during the complete sintering process was much higher in comparison to the higher heating rate. Higher energy results in increased mass transport and grain orientation between the particles. This effect could be observed from the SEM images shown in Fig. 6.6 where more diffusion between the particles can be seen in samples sintered at 2 ℃ /min as compared to 6℃ /min.

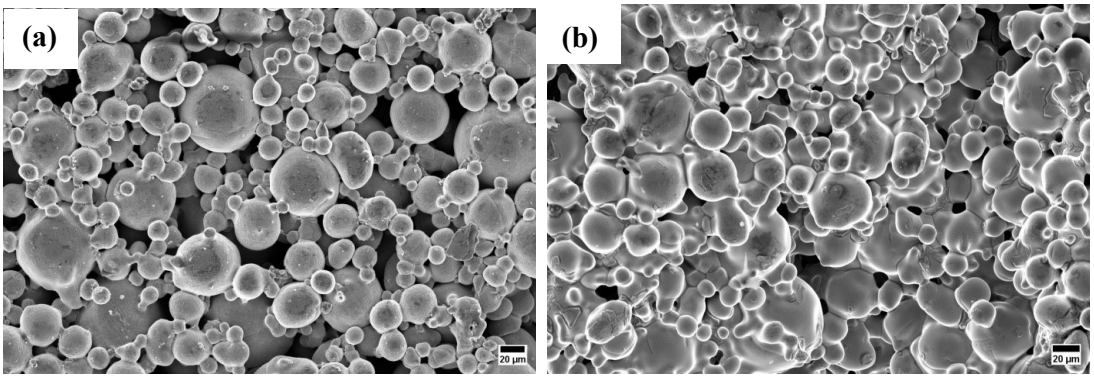

Fig. 6.6: SEM images of sintered samples at the sintering temperature of 950 ℃, a heating rate of 4 ℃ $/min$ and soaking time of a) 30 min b) 90 min

6.1.4.3 Effect of soaking time

It can be observed from the Fig. 6.4 that with the increase in soaking time the volumetric shrinkage is found to increase. This is due to the increased particle merging and mass transport. Moreover, at high values of soaking time significant time for diffusion is available that leads to increased densification and hence shrinkage.

6.1.4.4 Effect of interaction

The experimental findings reveal that the interaction between sintering temperature and heating rate plays a critical role in determining the extent of volumetric shrinkage. Specifically, at lower heating rates, the particles experience prolonged exposure to elevated temperatures, which allows for enhanced atomic diffusion. This extended diffusion time

facilitates greater energy absorption by the particles, thereby promoting more effective neck growth and densification. As a result, the porosity within the structure diminishes, leading to an increase in relative density. Consequently, the material undergoes more substantial volumetric shrinkage due to the collapse and elimination of pores during the sintering process.

6.1.5 Multi -Objective Optimization

The multi-objective optimization formulation was carried out to optimize relative density, volumetric shrinkage, and compressive yield strength. The global optimum solution was found using the genetic algorithm (GA) based multi-objective optimization approach. The optimization was performed using MATLAB 2017b's Optimization Toolbox. Since the toolbox is designed for minimization, the reciprocals of the original objective functions were used to convert the maximization problem into a minimization format. This allowed effective use of the Genetic Algorithm to optimize key responses such as relative density, compressive strength, and volumetric shrinkage within the defined constraints. Below are the goals and limitations for the multi-objective optimization.

$$Minimize\ f = \frac{1}{RD} + \frac{1}{\sigma_y} + V$$

Subject to condition.

$$650 \leq X_1 \leq 1050$$

$$2 \leq X_2 \leq 6$$

$$30 \leq X_3 \leq 90$$

Table 6.1 summarizes the optimized sintering parameters along with their corresponding values of relative density, compressive strength, and volumetric shrinkage.

Table 6.1 Optimized set of sintering parameters

Parameters				Relative density (%)		Compressive strength (MPa)		Volumetric shrinkage (%)	
S. No.	X_1	X_2	X_3	Statistical	Experimental	Statistical	Experimental	Statistical	Experimenta
1.	938	2	80	94.54±2.68	91.94	139.78±9.14	132.14	26 ±2.12	24.06

Table 6.1 summarizes the optimized sintering parameters along with their corresponding values of relative density, compressive strength, and volumetric shrinkage. The results demonstrate a well-balanced combination of high densification, improved mechanical strength, and controlled shrinkage, indicating the effectiveness of the selected parameters in enhancing the overall material performance. From Table 6.1, it can be inferred that a sintering temperature of 938℃ , heating rate of 2 ℃ /min and soaking time of 80 min are optimized parameters for post sintering of 3D printed green Cu electrode samples.

6.1.6 Proof of concept

After establishing the procedure for the development of high particle loading optimum Cu ink, 3D printing using DIW and thermal sintering, it becomes important to validate the established technology. Hence, a proof-of-concept case study on the fabrication of an HP-Cu structure using DIW and thermal sintering was performed. The optimum 97 wt % Cu ink was used to print the green sample and the DIW was performed using a 200 μm nozzle. Thereafter, the sintering was carried out using optimized parameters. The 3D printed Cu current collector for lithium metal battery shown in Fig. 6.7 reveals the successful fabrication of HP-Cu sample using the developed ink and processing route.

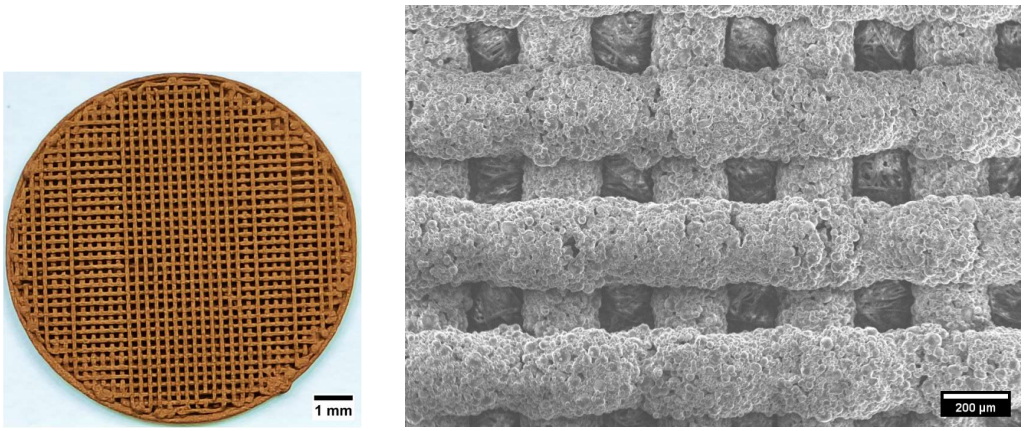

Fig. 6.7: Green sample of the porous Cu current collector with 97 $wt\%$ Cu loading

It may also be observed from Fig. 6.7, that the porous current collector has the pore size of 150 μm designed for improving the performance of the battery.

6.1.7 Compression Analysis

To verify the effectiveness of the developed process along with the optimized post-sintering parameters, a preliminary validation study was undertaken. In this study, a thin, porous Cu electrode was successfully fabricated, exhibiting a diameter of 16 mm and an average pore size of 154 ± 10 µm, thereby demonstrating the capability of the process for producing functional electrode structures. As part of the validation process, the fabricated sintered porous Cu electrode as shown in Fig.6.8 was utilized to construct a LMB in a coin cell configuration.

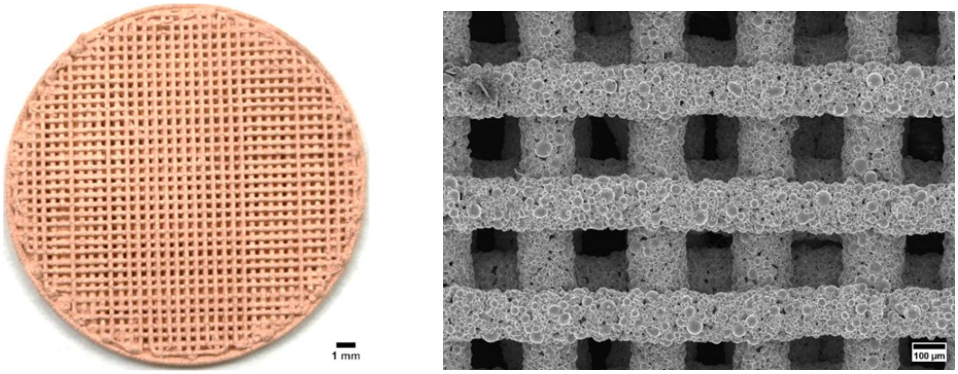

Fig. 6.8: Porous Cu current collector sintered sample printed with optimized printing parameters

This step was essential for assessing the electrode's suitability and performance under real-world conditions. The choice of a coin cell design facilitated a compact and controlled setup for evaluating the material's electrochemical and mechanical behavior in a simulated operational environment. A crucial aspect of this study was the evaluation of the mechanical robustness of the porous Cu electrode. In particular, the strength of the porous electrode is a key performance criterion, as electrodes in energy storage devices are frequently subjected to mechanical stresses during various stages of their lifecycle.

To address this challenge and ensure reliability, the fabricated sintered samples underwent testing under compression loading conditions as shown in Fig. 6.9.

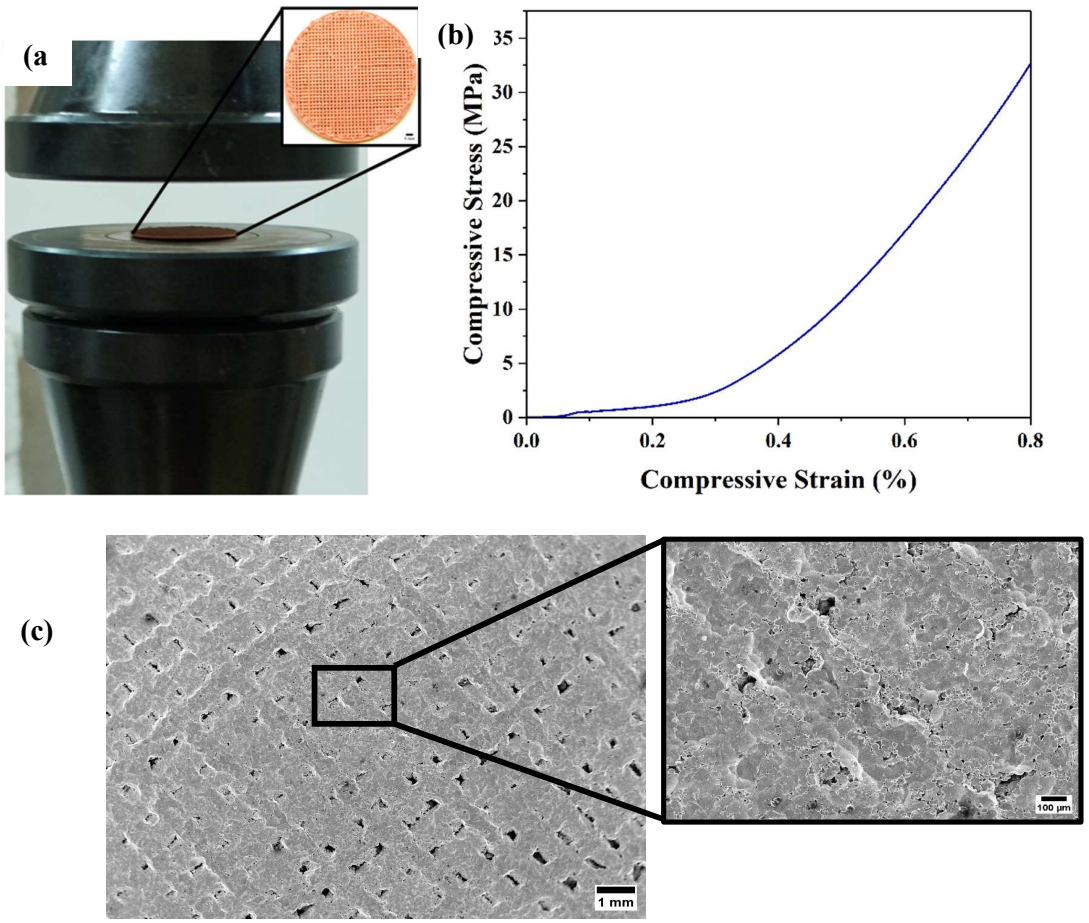

Fig. 6.9: a) Compression test of 3D printed porous Cu electrode b) Stress-strain plot for Cu electrode under compression (c) SEM image of the porous copper electrode after 80 % of straining

This testing was specifically designed to mimic the mechanical stresses experienced by the electrodes during assembly and operational use. By subjecting the samples to these conditions, the study aimed to validate the structural integrity and resilience of the optimized porous Cu electrode, providing confidence in its ability to withstand the demanding mechanical requirements of LMB applications.

Overall, this preliminary validation study not only highlights the capability of the developed process to produce finely porous, high strength Cu electrodes but also underscores its practical relevance in advancing the field of energy storage technology. The results establish a new benchmark for 3D-printed porous Cu electrodes and reinforce the importance of mechanical robustness in ensuring the long-term reliability and performance of LMBs.

The stress – strain graph was plotted for 3D printed $HP-Cu$ electrode as shown in Fig. 6.9 (b). The stress-strain curve for the compression test of a $HP-Cu$ current collector typically exhibits a behavior influenced by the material's porosity and its porous structure. At the initial stage of compression, the HP-Cu electrode exhibits elastic deformation, characterized by a linear increase in stress with strain. This is followed by a distinct plateau region, where the stress remains relatively constant over a range of strain. The plateau behavior is attributed to the progressive collapse and buckling of the porous architecture, which absorbs the applied load without a significant increase in stress. As the strain increases further, a sharp rise in stress is observed, indicating the onset of densification. This stress escalation corresponds to the elimination of pores and voids, as the structure transitions from a porous to a fully compacted state. The limited increase in strain during this phase suggests that the material has reached near-complete densification, effectively behaving as a solid. This transition is clearly evident in the SEM image shown in Fig. 6.9(c). Notably, even under 80% compressive strain, the HP-Cu electrode did not exhibit any signs

of fracture, as confirmed by high-magnification SEM imaging, underscoring its excellent mechanical integrity and structural robustness. Hence, it could be established that the fabricated porous Cu current collector has sufficient mechanical integrity to be used for metal battery applications.

Figure 6.10 represents a two-part analysis related to the performance of a 3D-printed porous copper current collector.

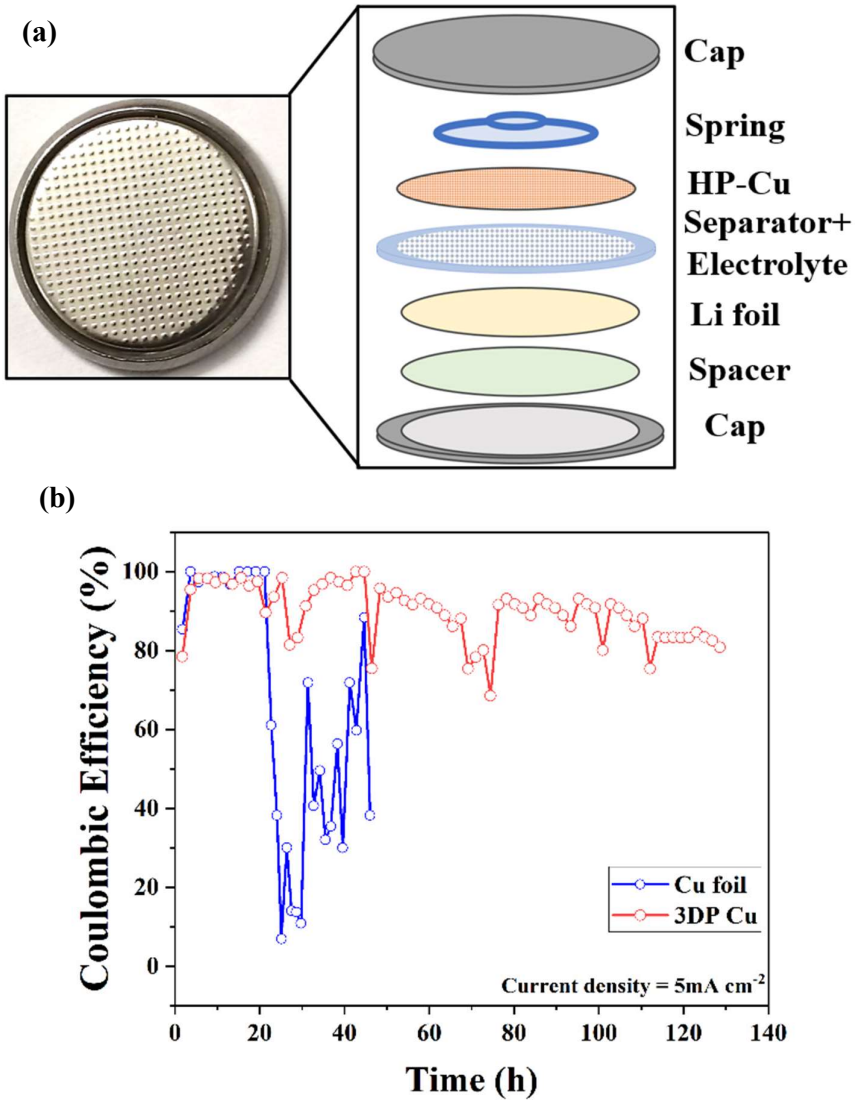

Fig. 6.10: a) Schematic of 3D printed porous Cu current collector b) Comparison of Coulombic efficiency of fabricated coin cell and Cu foil at current density of 5 $mAcm^{-2}$ for the plating capacity of 5 $mAhcm^{-2}$

Fig. 6.10 (a) shows a schematic of the 3D-printed porous Cu structure, illustrating its designed architecture aimed at enhancing electrochemical performance through increased surface area and improved ion transport pathways. Fig. 6.10 (b) provides a comparative evaluation of the Coulombic efficiency between a coin cell incorporating the 3D-printed porous Cu collector and one using conventional Cu foil. This comparison was conducted at a current density of 5 mA·cm⁻² with a plating capacity of 5 mAh·cm⁻².

The results highlight the improved efficiency and stability of the 3D-printed collector under high current density conditions, demonstrating its potential advantages for use in lithium metal batteries. the current density of 5 $mAcm^{-2}$ at plated capacity of 5 $\mathrm{mAhcm^{-2}}$. Fig. 6.10 (b) shows the 3D- printed HP-Cu current collector exhibiting the highest coulombic efficiency of 90.14 % for more than 100 h.

Moreover, Fig. 6.10 (a) illustrates that the 3D printed HP-Cu current collector exhibited a steady cycle with minimum variation. This may attribute inhibiting the growth of dendrites at battery anode. On the other hand, it has been found that the coulombic efficiency of Cu foil was 42.46 % and it decreases quickly after 20 h. The low value of coulombic efficiency may be caused by dendritic growth, which increases the risk of the battery shorting out. It can also be observed from the Fig. 6.10 that the efficiency of the Cu foil was varying between 15 to 90 %, and as the number of cycles was increasing there was sharp fall in coulombic efficiency after 20 h. It can be attributed that the cycle of the Cu foil is unstable as compared to 3D printed porous Cu current collector. The sharp fall in coulombic efficiency of the Cu foil was attributed to formation of dendrites and volume expansion. Moreover, for the current density of 5 $\mathrm{mAcm^{-2}}$, the 3D-printed HP-Cu current collector exhibited more stability as compared to Cu foil. The 3D-printed HP-Cu current collector was more stable even after 100 h whereas Cu foil cycle was unstable after 15 h at 5 $\mathrm{mAcm^{-2}}$. Following the optimization of both printing and sintering parameters,

morphological characterization becomes a critical step in evaluating the structural integrity and quality of the fabricated HP-Cu components. Detailed morphological analysis plays a vital role in assessing the effectiveness of the processing route in mitigating issues such as the formation of dendrites, which can severely impact the performance and reliability of electrochemical devices. The microstructural features including pore distribution, particle connectivity, and surface topology provide essential insights into how well the optimized parameters contribute to achieving a stable and uniform porous structure. To this end, the subsequent chapter presents a comprehensive discussion of both the electrochemical performance and the morphological characteristics of the sintered HP-Cu samples. This integrated evaluation is aimed at establishing a clear correlation between the material's structural features and its functional behavior in energy storage applications.